

## A GEOMETRIC SAMPLING THEOREM AND ITS APPLICATION IN MORPHOLOGICAL IMAGE CODING

Guillermo Sapiro and David Malah

Technion - Israel Institute of Technology  
Department of Electrical Engineering  
Haifa 32000, Israel

This paper deals with reconstruction properties of the skeleton representation, presents a *Geometric Sampling Theorem (GST)*, and describes an approach for gray level image coding based on it and on binary morphological operations. The theorem states conditions for the reconstruction of the boundary of a *continuous* two level image from a *unique* subset of points of its skeleton representation. This set of points, called *singular points*, plays an important role in the skeleton representation of *discrete* binary images as well. The coding scheme consists of the following steps: First, the image is pre-processed by an error-diffusion technique. The pixel values are subsequently converted to Gray-code. The bit-planes are represented by a *modified morphological skeleton* which uses an *increasing size* structuring element. Redundancy in this representation is reduced with an algorithm motivated by the *GST*. These *reduced modified morphological skeletons* are coded with an entropy coding scheme particularly devised for efficient skeleton coding.

### 1. INTRODUCTION

Medial axis and skeleton representations have received much attention; both in theoretical [1-4], and in practical aspects [5]. This paper concentrates on reconstruction properties of the skeleton, and presents a *Geometric Sampling Theorem (GST)*. The theorem deals with the representation, via a skeleton subset, of sets in the continuous two dimensional space  $R^2$ . In the second part of the paper, an approach for gray-scale image coding is described [6], which is based on the *GST* and on a *modified morphological skeleton* which uses an *increasing size* structuring element instead of a fixed size element as in [5].

The *GST* states conditions for the reconstruction of the boundary of a *continuous* two level image (i.e. a set of  $R^2$ ) from a *unique* subset of points of its skeleton representation. We describe this set of points, called *singular points*, along with some of their properties. Analogy between this theorem and the classical Sampling Theorem is given as well. In the case of discrete binary images (i.e. sets of  $Z^2$ ), we found that the singular points of the discrete skeleton convey most of the information required for reconstruction. Based on this fact, we develop an algorithm for efficient computation of the *minimal skeleton* of discrete binary images (i.e. a subset of the skeleton whose points are sufficient for exact reconstruction).

The approach used for image coding is as follows: The image is first pre-processed by an error dif-

fusion technique in order to reduce the number of bit planes, without significant quality degradation. The pixel values are subsequently represented in Gray-code, in order to obtain more uniform bit-planes. These bit-planes are represented each by means of a *modified morphological skeleton*, and redundancy in this representation is reduced using an algorithm based on the *GST*. These skeletons, which are sparse representations of the bit-planes, are coded with a combination of different entropy coders particularly devised for efficient skeleton coding.

The following sections give the proof of the *GST* and details of the coding algorithm along with processed examples. Section 2 introduces the skeleton and presents the *GST*. Section 3 describes the *modified morphological skeleton*. In section 4, description of the coding algorithm is given. Experimental results are presented in section 5, and a summary and conclusions in section 6.

*Notation:*  $A \ominus B$ ,  $A \oplus B$ ,  $A \circ B$ , and  $\bar{A} \bullet B$  denote the basic morphological operations of erosion, dilation, opening, and closing, respectively, of a set  $A$  by the *structuring element*  $B$ . Both  $A$  and  $B$  are sets in  $R^2$  or in  $Z^2$  [1].

### 2. MORPHOLOGICAL SKELETON AND A GEOMETRIC SAMPLING THEOREM

Let  $X$  be a closed set in  $R^2$ . The curvature  $\kappa(p)$  at a point  $p$  of the boundary  $\partial X$  of the set  $X$  is

defined as the inverse of the radius of the largest disk tangent to  $\partial X$  at  $p$  [1]. We assume that the Convex Hull of  $X^c$  is equal to  $R^2$  (a necessary condition for the exact reconstruction of  $X$  [1-4]) and that  $\kappa(\cdot)$  of  $\partial X$  is well defined everywhere, except at a finite number of points, where it may have only one sided tangents. We denote these set of boundary points by  $\Gamma(X)$ ,  $\Gamma(X) \subset \partial X$ . The subset of points in  $\Gamma(X)$  for which the correspondent interior angle is concave (e.g., the points  $B, F$  in Figure 1) is denoted by  $\xi(X)$ . We also define  $Y_\rho = X \circ \rho B$ , where  $B$  is the unit disk in  $R^2$ .

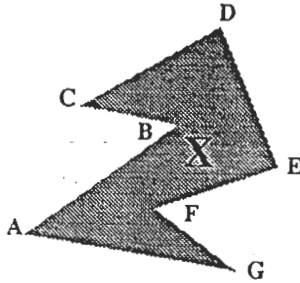


Fig. 1: Points with no well defined curvature:  
 $\Gamma(X) = \{A, B, \dots, G\}$ ,  $\xi(X) = \{B, F\}$ .

Let  $D(x, \rho)$  be a closed disk of center  $x$  and radius  $\rho \geq 0$  (in a two-dimensional Euclidian space). Then, a maximal disk in  $X$  and the skeleton of  $X$  are defined as follows:

**Maximal Disk:** A maximal disk  $D(\psi, \rho_\psi)$  is one which is included in the object  $X$ , but not included in any other disk in  $X$ .

**Skeleton in  $R^2$ :** The skeleton  $\Psi(X)$  of an object  $X \subset R^2$  is defined as the family of centers of all maximal disks in  $X$  [1-4, 7].

If  $\psi \in \Psi(X)$ , then  $D(\psi, \rho_\psi)$  denotes its corresponding maximal disk with radius  $\rho_\psi$ , i.e.  $\rho_\psi$  is the Euclidian distance from  $\psi$  to  $\partial X$ .

It is well known [1-4] that under the assumed conditions,  $X$  can be reconstructed from the set  $\Psi(X)$  together with the set of radii  $\rho_\psi$ , i.e. the skeleton pairs  $(\psi, \rho_\psi)$ :

$$X = \bigcup_{\psi \in \Psi(X)} D(\psi, \rho_\psi) \quad (1)$$

Not all skeleton points are necessarily needed for exact reconstruction. We are interested in a set of points  $\Psi_m(X) \subset \Psi(X)$ , denoted as the *minimal skeleton*, which guarantees exact reconstruction of  $X$ , and which satisfies the condition that  $X$  can not be recovered from any subset of  $\Psi_m(X)$ . Such a set exists, because in the worst case  $\Psi_m(X) = \Psi(X)$ . Similarly, we are interested in the minimal set for recovering  $\partial X$ .

For demonstration, Figure 2 shows a set in  $R^2$  with its skeleton. In this case just the two marked points  $\{a, b\}$ , together with their corresponding radii  $\{\rho_a, \rho_b\}$ , are sufficient for object reconstruction.

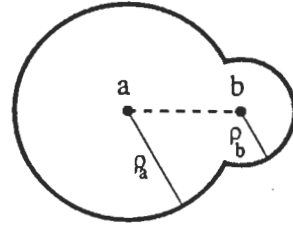


Fig. 2: Example of skeleton (dashed line) and minimal skeleton (points  $a, b$ ):  $\Psi_m(X) = \{a, b\}$ .

Before proceeding, we define the following:

**Singular Point:** A skeleton point  $s$ ;  $s \in \Psi(X)$ , is a *singular point* if and only if there exists a point  $p$  in  $X$  such that the maximal disk  $D(s, \rho_s)$  is the only one which contains it.

Also, for any point  $s \in \Gamma(X) \setminus \xi(X)$ ,  $s$  is singular with maximal disk  $D(s, \rho_s)$  where  $\rho_s = 0$  (see for example points  $A$  and  $D$  in Figure 1)

Let  $S(X)$  be the unique set of singular points in  $X$  and let  $X^*$  the *minimal reconstruction* defined by:

$$X^* = \bigcup_{s \in S(X)} D(s, \rho_s) \quad X^* \subset X \quad (2)$$

**Boundary Singular Point:** Similarly, we say that a point  $x \in \psi(X)$  is a *boundary singular point*, if and only if there exists a point  $p$  on  $\partial X$  (the boundary of  $X$ ) such that the maximal disk  $D(x, \rho_x)$  is the only one which contains it.

In the case of the set in Figure 2, the two marked points  $a, b$  are singular and  $\Psi_m(X) = S(X)$ . The importance of singular points is evident from this example and from the following theorems.

**Lemma 1:** All singular points are in  $\Psi_m(X)$ , i.e.,  $S(X) \subset \Psi_m(X)$ .

*Proof:* This is a direct consequence from the definition of a singular point. □

**Theorem 1:**  $x \in X$  is a *boundary singular point* if and only if  $x$  is a singular point.

*Proof:*

$\Rightarrow$  From the definitions, if  $x$  is boundary singular, then  $x$  is singular.

$\Leftarrow$  Given a singular point  $x$ , we have to prove that  $x$  is boundary singular:

For all  $z \in \Psi(X)$ ,  $D(z, \rho_z) \cap \partial X \neq \emptyset$  (Figure 3). If  $D(z, \rho_z)$ , with  $z \in \Psi(X)$  and  $\rho_z > 0$ , touches  $\partial X$

only at points with *not* well defined curvature, i.e.  $D(z, \rho_z) \cap \partial X \subseteq \xi(X)$ ; then it can not be a singular point. Therefore, for any singular point  $x \in \Psi(X)$ , its corresponding maximal disk  $D(x, \rho_x)$  touches the object boundary at least at one point  $A_x$ , such that  $A_x \in D(x, \rho_x) \cap \partial X$  and  $A_x \in \partial X \setminus \xi(X)$ . If we prove that  $D(x, \rho_x)$  is the only maximal disk which contributes to  $A_x$ , then  $x$  is also a boundary singular point.

Lets prove now that  $D(x, \rho_x)$  is the only maximal disk which touches  $\partial X$  at  $A_x$ , when  $\kappa(A_x)$  is well defined. We have to show that there is no other  $y \in \Psi(X)$ ,  $x \neq y$ , such that  $A_x \in D(y, \rho_y) \cap \partial X$ . Suppose such a  $y$  do exists. Since the curvature  $\kappa(A_x)$  is well defined, then both  $D(x, \rho_x)$  and  $D(y, \rho_y)$  are tangent to  $\partial X$  at  $A_x$ ; and  $x, y \in N_{A_x}$ , where  $N_p$  stands for the normal to  $\partial X$  at a point  $p \in \partial X$  with  $\kappa(p)$  well defined. This means that  $D(x, \rho_x)$  and  $D(y, \rho_y)$  are nested disks (see Figure 3), a contradiction to the hypothesis that they are maximal disks ( $x, y \in \Psi(X)$ ). Then,  $D(x, \rho_x)$  is the only maximal disk which contains  $A_x \in \partial X$ , and  $x$  is a boundary singular point. □

This theorem means that a singular skeleton point contributes to  $X$  if and only if it contributes to  $\partial X$ . Therefore, when checking for the singularity of a point, just the intersection points of its corresponding maximal disk with the set boundary need to be checked.

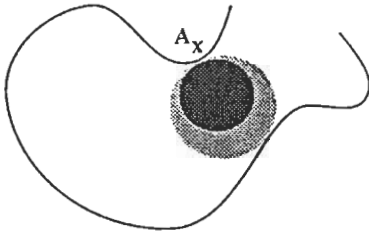


Fig. 3: Nested circles, only one can be maximal.

**Theorem 2 - The Geometric Sampling Theorem:**

- a)  $X^*$  covers all the  $X$  boundary ( $\partial X$ ), except for a finite number of points.
- b) The subset of  $S(X)$  containing singular points with corresponding radii  $r \geq \rho$ , is enough for reconstruction of all of  $Y_\rho$  boundary, except for a finite number of points (these points are the same as in the first part of the theorem).

*Proof:*

- a) Any boundary point  $A_x \in \partial X$  belongs to at least to one maximal disk  $D(x, \rho_x)$  (eqn. (1)),  $x \in \Psi(X)$ .

In the proof of Thm. 1 we showed that if  $\kappa(A_x)$  is well defined, then  $x$  is a singular point (or a boundary singular point). Therefore,  $X^*$  covers at least all the boundary points with well defined curvature, i.e.  $\partial X \setminus \xi(X)$ , and the number of uncovered points is at most  $\#\xi(X) < \infty$ .

For coverage of the uncovered points (a subset of  $\xi(X)$ ), the number of skeleton points that must be added is less or equal than  $\#\xi(X)/2$ .

- b) This is a direct consequence from the first part of the theorem and from the fact that 
$$Y_\rho = \bigcup_{\psi \in \Psi(X), \rho_\psi \geq \rho} D(\psi, \rho_\psi).$$

□

From the above two theorems we see the importance of the unique set  $S(X)$  for the reconstruction of  $X$ , since each singular point contributes to  $\partial X$  and almost all of  $\partial X$  is covered by the maximal disks of  $S(X)$ . By the second part of Thm. 2 one is motivated to denote the morphological operation  $X \circ \rho B$  as a *geometric low pass filter*, in analogy to the filter used in classical signal processing, with band-width being replaced here by the inverse of the radii of maximal disk.

When  $X$  is opened by  $\rho B$  (yielding  $Y_\rho$ ), arcs of the skeleton are eliminated. Lower bounds on the length of these arcs are given in [8].

For an extension of the theorems, and an extended analysis of the analogy between this theorems and the classical Sampling Theorem, see [8].

### 3. MORPHOLOGICAL SKELETON OF DISCRETE IMAGES

The skeleton  $SK^B(X)$  of a *discrete* set  $X$  (a subset in  $Z^2$ ) can be defined in a similar way in which the skeleton of a continuous set is defined. This skeleton is defined in relation with a *discrete structuring element*  $B$ , which replaces the disk used in the continuous case. Thus, the discrete skeleton is defined as follows:

**Maximal Structuring Element:** If  $(nB)_z$  represents the subset obtained after dilating  $B$   $n$ -times and shifting the result by  $z$ , then the element  $(nB)_z$  is maximal if and only if it is included in  $X$  and there is no other  $(mB)_y$ ,  $m > n$ , such that  $(nB)_z \subset (mB)_y \subset X$  [1, 5].

**Skeleton in  $Z^2$ :** The skeleton  $SK^B(X)$  of a set  $X \subset Z^2$  is defined as the family of centers of all maximal structuring elements in  $X$  [5].

Lantuejoul [7] proved that the skeleton can be computed via basic morphological operations. We present the discrete version of the algorithm, as was

used by Maragos and Schafer in [5] for binary image coding. Assume  $X$  to be a discrete set, and  $B$  a discrete structuring element (i.e. sets in  $Z^2$ ), then the skeleton  $SK^B(X)$  is given by [1, 5]:

$$SK^B(X) = \bigcup_{n=0}^{N(B)} S_n^B(X) \quad (3)$$

where

$$S_n^B(X) = (X \ominus nB) - (X \ominus nB) \circ B, n=0, \dots, N(B) \quad (4)$$

The subset  $S_n^B(X)$  is called the  $n$ -th skeleton subset of  $X$ , computed with the structuring element  $B$ , and  $N(B) = \max\{n : X \ominus nB \neq \emptyset\}$ . The  $n$ -th skeleton subset  $S_n^B(X)$  contains all the points  $x \in X$  (and only those points), such that the element  $(nB)_x$  is maximal in  $X$ .

Opened versions of  $X$  can be obtained via:

$$X \circ kB = \bigcup_{n=k}^{N(B)} S_n^B(X) \oplus nB \quad (5)$$

where  $0 \leq k \leq N(B)$ . Hence, if  $k=0$  the original image is reconstructed.

The morphological skeleton just presented is computed via the structuring element  $B$ , with invariant shape and size. We propose next a new morphological skeleton, for which the structuring element size increases with subsequent skeleton steps ( $n$ ) (the shape remains unchanged). This new representation is motivated by the fact that when larger structuring elements are used, less skeleton subsets are obtained; enabling this way a higher compression ratio (see next section). In the modified morphological skeleton of  $X$ , each skeleton subset is computed with the largest possible structuring element; i.e. an element  $kB$  such that if  $Y = X \circ kB$ , then  $Y \circ kB = Y$  and  $Y \circ (k+1)B \subsetneq Y$ . From equation (5) we see the following:

$$X = X \circ B + S_0^B(X) \quad (6)$$

and

$$X \circ 2B = X \circ 2B + S_1^B(X) \oplus B \quad (7)$$

Now, we can decompose  $X \circ 2B$  in a different way:

$$\begin{aligned} X \circ 2B &= \bigcup_{n=1}^{N(2B)} S_n^{2B}(X) \oplus n2B = \\ &= X \circ 4B + S_1^{2B}(X) \oplus 2B \end{aligned} \quad (8)$$

Where  $S_n^{2B}(X)$ ,  $n = 1, 2, \dots, N(2B)$ , are the skeleton subsets of  $X$  computed with the structuring element  $2B$  (note that the union goes from  $n=1$ ).

We therefore can rewrite eqn. (6) as:

$$X = X \circ 4B + S_1^{2B}(X) \oplus 2B + S_1^B(X) \oplus B + S_0^B(X) \quad (9)$$

Subsequently,  $X \circ 4B$  can be decomposed using  $4B$  as a structuring element and this procedure can be continued using at each step a twice as big structur-

ing element as in the previous step. We obtain this way the *modified morphological skeleton*  $MS(X)$  [8]:

$$MS(X) = \bigcup_{n=0}^{N_M(B)} M_n(X) \quad (10)$$

where

$$M_0(X) = S_0^B(X) \quad (11a)$$

$$M_n(X) = S_1^{B(n)}(X), n = 1, \dots, N_M(B) \quad (11b)$$

$$B(n) = \begin{cases} \{(0,0)\} & n = 0 \\ 2^{n-1}B & n = 1, \dots, N_M(B) \end{cases} \quad (11c)$$

The skeleton subset  $M_n(X)$  contains all the points  $x \in X$  (and only those points) such that the element  $(2^{n-1}B)_x$  is maximal in  $X$ ; and  $N_M(B) = \max\{n : X \ominus 2^{n-1}B \neq \emptyset\}$ . We observe that with this modified morphological skeleton, less skeleton subsets are obtained due to the use of an increasing size structuring element, since  $N_M(B) = \lceil \log_2 N(B) \rceil < N(B)$ .

The image can be reconstructed from the modified morphological skeleton as follows:

$$X \circ kB = \sum_{n=k}^{N_M(B)} [M_n(X) \oplus B(n)] \quad (12)$$

where  $0 \leq k \leq N_M(B)$ . Hence, if  $k=0$  the original image is reconstructed (see eq. (11)). More details about this modified morphological skeleton are given in [8].

#### 4. IMAGE CODING

Figure 4 presents the block diagram of the coding algorithm. We describe in this section each of the stages. More details can be found in [6].

The image is first pre-processed in order to represent it in a new form, more appropriate for our coding method. The first step in the pre-processing stage reduces the number of bit planes from 8 to 4 via the Floyd-Steinberg error diffusion algorithm [9]. With this technique we eliminate the least significant bit-planes of the 8-bit image, which due to their random-like structure, are typically difficult to compress. Thus, using 4 bit planes with error diffusion, the compression ratio is increased with no significant degradation. Subsequently, pixels in these bit-plane are represented in Gray-code, obtaining more uniform bit-planes which improves the coding algorithm performance.

Each one of the four bit-planes obtained after the pre-processing stage is represented by means of the *modified morphological skeleton* described in

the previous section (equations (10)-(12)). We use a  $3 \times 3$  square as the basic structuring element ( $B$ ). Usually, no more than 6 skeleton subsets were obtained for the different bit-planes ( $N_M(B)=5$ , see eqn. (10)).

The *modified morphological skeleton* is still a redundant representation in such a way that some skeleton points can be removed and exact reconstruction of the image from the reduced morphological skeleton can still be obtained. Our approach for removing redundant skeleton points is based on the algorithm presented in [5] and improved by using results from the Geometric Sampling Theorem described in the previous section. A dual geometric sampling theorem for discrete images does not exist. However, we found that the *singular points* of a discrete skeleton (defined in a similar way as the singular points of a continuous one), are not sufficient for exact image reconstruction, but they do reconstruct most of it (typically close to 90%). Therefore, the set of singular points is almost sufficient; and we have to care about the "optimal" coverage of only a small part of the image (typically 10%) instead of the optimal coverage of the whole image as needed in [5]. The resulting *search space* is much smaller than the original one, and a solution closer to the optimal one can be found with simpler methods. We decided to select the skeleton points, needed in addition to the singular points, according to the contribution of their corresponding maximal element to the partial reconstructed image (see equations (1), (5), and (12)). We denote by  $M'_n(X)$  the reduced skeleton subset obtained from  $M_n(X)$ . We obtain this way that each of the bit-planes is being completely represented by its *reduced modified morphological skeleton (RMMS)*.

Before proceeding with coding the *RMMS*, we point out that simulation results suggest that a discrete version of Thm. 1 may be valid. Therefore, when checking for the singularity of a point, it is enough to check its boundary contribution, thereby reducing the computational complexity of the presented skeleton reduction approach (this complexity is *linear* in the maximal structuring element size instead of *quadratic* as in [5]).

For coding the *RMMS* representation of each bit-plane, each skeleton subset  $M'_n(X)$  is coded as a binary image (these are very sparse binary images). First, a Huffman code of the number of consecutive empty lines (lines having no skeleton points) is generated, from which the exact position of non-empty lines can be pointed out. The position of each skeleton point in its corresponding non-empty line, is coded by an Elias code as proposed in [5]. The binary output of the Elias code (of all skeleton subsets combined) is compressed with the Ziv-Lempel universal coding algorithm.

This coding strategy was found to be very efficient for *RMMS* coding, because of their special structure as mentioned above. An improvement in the compression ratio was obtained using the *RMMS* representation instead of the original morphological skeleton representation proposed by Maragos and Schafer [5], mainly due to the reduction in the amount of bits needed for coding the empty lines.

By introducing geometrical errors in the different bit-planes, the compression ratio can be increased. These errors correspond to the omission of *RMMS* subsets  $M'_n(X)$ ,  $n < r \leq N_M(B)+1$ , where  $r$  is selected according to the bit-plane importance (for more significant bit-planes,  $r$  is small or even zero); obtaining with this method smoothed versions of the form  $X \circ B(r)$  of the bit-planes (equation (12)). If just the smoothed bit-plane is coded, missing points of  $X$  ( $X \circ B(r) \subseteq X$ ) would appear in the reconstruction as part of the background. This causes considerable degradation of the subjective image quality. To circumvent this problem, we code the smoothed versions of both  $X$  and its complement,  $X^c$ , and subsequently fill-in randomly the undefined regions or "holes" (Fig. 5d).

Skeleton subsets that were initially omitted can be progressively added in subsequent steps until the image quality is satisfactory, or the desired bit-rate is achieved. We denote this procedure as *Geometric Progressive Transmission* [6].

## 5. SIMULATION RESULTS

To evaluate the performance of the proposed coding scheme, it was simulated on a SUN 4/260, using a Gould IP8500 image display system. A woman's head and shoulder image ("Lena") of size  $512 \times 512$  pixels was used as a test image (for more examples see [8]). Performance of the algorithm is evaluated based only on the subjective quality of the images.

Fig. 5a shows the original image. Fig. 5b shows the image represented using only four bit-planes with error-diffusion. This image was coded (using the *RMMS*) at the rate of 0.35 bits per pixel (b/p), and represents what we call the "Four-bit error-free image". The same picture, when represented via the morphological skeleton proposed in [5] (instead of the *RMMS*) is coded at the rate of 0.40 b/p. Fig. 5c shows an image that was initially filtered with a  $3 \times 3$  median filter followed by 4-bit error-diffusion. This image was coded at 0.29 b/p. Fig. 5d shows the reconstruction of an image in which the least significant bit-plane (of the 4-bit error-diffusion representation) was coded with no skeleton points of radii zero; both the image and the background were coded and "holes" were filled randomly (the remaining bit-planes were coded error-free). This image required 0.29 b/p.

## 6. SUMMARY AND CONCLUSIONS

In this paper a *Geometric Sampling Theorem (GST)* is presented. The theorem deals with the reconstruction of the boundary of a *continuous* two level image from a *unique* subset of points of its skeleton representation. This set of points, called *singular points*, was found to play an important role in the skeleton representation of *discrete* binary-image as well. Based on this fact, an efficient algorithm for morphological skeleton reduction was proposed.

A *modified morphological skeleton* for binary image representation is also presented. This skeleton is computed with an *increasing size* structuring element. This way, the number of skeleton subsets is reduced and therefore the compression ratio is increased.

In the second part of the paper, an approach for morphological image coding was described. The image is first reduced from 8-bits to 4-bits via an error-diffusion algorithm, and the pixels are subsequently converted to Gray-code. The resulting bit-planes are represented via the *modified morphological skeleton*. Redundancy in the representation is reduced via an algorithm which is based on the *GST*. An entropy coding scheme was particularly devised for efficient coding of these skeletons. This coding scheme is quite different from morphological approaches which are based on image segmentation and labeling (e.g., [10]). Also, the error introduced by geometric deformations is in general more pleasant to the observer than the blocking or quantization errors introduced by standard image coding algorithms.

## REFERENCES

- [1] J. Serra, *Image Analysis and Mathematical Morphology*, Academic Press, 1982
- [2] J. Serra, Editor, *Image Analysis and Mathematical Morphology-Volume 2: Theoretical Advances*, Academic Press, 1988
- [3] H. Blum, "Biological Shape and Visual Science", *J. Theor. Biol.* 38, pp. 205-287, 1973
- [4] L. Calabi and W. E. Hartnett, "Shape Recognition, Prairie Fires, Convex Deficiencies and Skeletons", *Am. Math. Mon.* 75, 335-342, 1968
- [5] P. A. Maragos and R. W. Schafer, "Morphological Skeleton Representation and Coding of Binary Images", *IEEE Transactions of ASSP*, vol. ASSP-34, No. 5, pp. 1228-1244, October 1986
- [6] G. Sapiro and D. Malah, "Morphological Image Coding via Bit-plane Decomposition and a New Skeleton Representation", *Proc. of the 17th IEEE Convention of Electrical and Electronics Engineers in Israel*, May 1991
- [7] C. Lantuejoul, *La squelettisation et son application aux mesures topologiques des mosaïques polycristallines*, these de Docteur-Ingenieur, School of Mines, Paris, France, 1978
- [8] G. Sapiro, *Image Coding via Morphological Techniques*, M.Sc. Thesis, Technion, Israel Institute of Technology, Dept. of Electrical Engineering, 1991, in preparation
- [9] R. Ulichney, *Digital Halftoning*, MIT Press, 1987
- [10] S. A. Rajala, H. A. Peterson, and E. J. Delp, "Binary Morphological Coding of Gray-scale Images", *ISCAS'88*, pp. 2807-2811, 1988

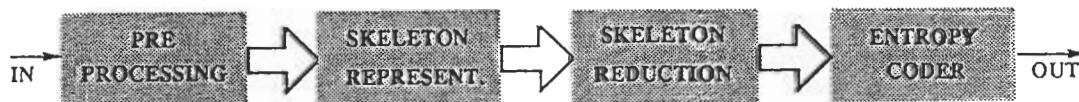


Fig. 4 - Block diagram of the coding scheme.



Fig. 5